2D TM scattering problem for finite dielectric objects in a dielectric stratified medium employing Gabor frames in a domain integral equation

The 2D TM scattering problem for finite dielectric objects in a dielectric stratified medium employing Gabor frames in a domain integral equation

ROELAND J. DILZ[1,*], MARK G. M. M. VAN KRAAIJ[2], AND MARTIJN C. VAN BEURDEN[1]

[1] Eindhoven University of Technology, P.O. Box 560, 5600MB, Eindhoven, The Netherlands
[2] ASML, De Run 6501, 5504DR, Veldhoven, The Netherlands
[*] Corresponding author: r.dilz@tue.nl

Compiled June 20, 2017

We present a method to simulate two-dimensional scattering by dielectric objects embedded in a dielectric layered medium with transverse magnetic polarization through a domain integral equation formulation. A mixed spatial-spectral discretization is employed with both a spatial and a spectral representation along the direction of the layer interfaces. In the spectral domain, a discretization on a path through the complex plane is used on which the Green function is well behaved. To calculate the field-material interaction in the spatial domain, an auxiliary field is employed similar to the Li factorization rules. Numerical results show that this auxiliary-field formulation significantly improves the accuracy, compared to a formulation that directly employs the electric field.

OCIS codes: *(050.1755) Computational electromagnetic methods; (050.2770) Gratings; (130.2790) Guided waves.*

http://dx.doi.org/10.1364/ao.XX.XXXXXX

1. INTRODUCTION

The simulation of electromagnetic scattering from finitely sized dielectric objects in a multilayered dielectric medium has several important applications. Among these applications are metrology for integrated-circuit production [1], metamaterials [2], and elements on nanophotonic chips [3]. Fast and accurate numerical methods are very important in these fields of research.

In a preceding article [4], we proposed a method to calculate the scattering from a two dimensional dielectric object illuminated by a wave with transverse electric (TE) polarization in a layered medium. We used a domain integral equation to solve the scattering problem. There are two key ingredients to this method. The first is the use of a Gabor frame as a discretization, which ensures a fast and exact Fourier transform. The second key ingredient is the use of a specially chosen path through the complex plane in the spectral domain on which we discretize the fields. On this path we are able to mitigate the poles and branchcuts that are present in the Green function.

In this article we show that the same ingredients can also be used for solving 2D scattering problems with Transverse Magnetic (TM) polarization. The challenge with TM polarization is that the electric field is discontinuous wherever the contrast function is discontinuous. After Lalanne and Granet discovered a method to accurately calculate the TM-polarized scattering from an object [5, 6], Li put this into a rigorous framework [7], which resulted in the so-called Li factorization rules. The key point of these articles is that when two functions with discontinuities at the same spatial position are approximated by a Fourier series, the product of the Fourier series does not converge well. Lalanne [5] solves the issue by replacing the discontinuous contrast operator by the inverse of a truncated inverse contrast operator. Granet [6] avoids the multiplication of functions with discontinuities at the same positions altogether by a reformulation. The way Granet handles spatial discontinuites can also be applied in the differential method formulation, where a generalization to more arbitrary shapes in three dimensions exists as the normal-vector field formulation [8, 9]. This class of methods to handle spatial discontinuites is not unique to each spectral method, they are applicable to many different spectral methods such as the Rigorous Coupled-Wave Analysis (RCWA) also known as the Fourier Modal Method [10, 11], the periodic Volume Integral Method (pVIM) [12, 13] and the Differential method [14].

We show that slow convergence of multiplications of functions with discontinuities at the same positions is also an issue when functions are represented by Gabor coefficients. However, following [6] we replace the electric field by an auxiliary field that is continuous. Multiplication of the discontinuous contrast function with this continuous auxiliary field yields a well-converging solution similar to the periodic case in [6].

We use two validation cases to demonstrate that this spatial-spectral approach yields accurate results.

2. FORMULATION

A. Problem description

Consider a two-dimensional dielectric object of finite size, described in the x-z plane by its relative permittivity function $\varepsilon_r(x,z)$. This dielectric object is embedded in one layer of a multilayered medium defined by $N-1$ layers with dielectric constants $\varepsilon_{rb,n}$ in the region between z_n and z_{n+1} and thickness $d_n = z_{n+1} - z_n$. This is illustrated in Figure 1. Above the top layer there is vacuum $\varepsilon_{rb,0} = 1$ and below the lowest layer there is a halfspace with relative permitivity $\varepsilon_{rb,N}$. We assume that the dielectric object is completely embedded in layer i. We define the contrast function $\chi(x,z)$ by

$$\chi(x,z) = \frac{\varepsilon_r(x,z)}{\varepsilon_{rb,i}} - 1, \tag{1}$$

which is nonzero only on the object. The simulation domain with bounds $-W \le x \le W$ and $z_i \le z_{min} \le z \le z_{max} \le z_{i+1}$ contains the dielectric object completely.

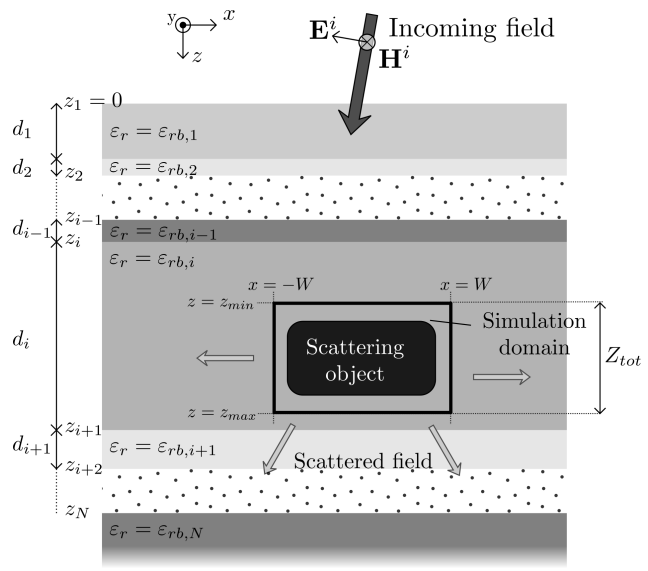

Fig. 1. Scattering setup. A TM polarized field is incident on a dielectric object located in layer i of a multilayered background medium.

We define the incoming field $\mathbf{E}^i$ as the field on the multilayer medium in abscence of the scatterer. This field has transverse magnetic (TM) polarization, i.e. its magnetic field $\mathbf{H}^i$ is directed in the transverse y direction, so the $\mathbf{E}^i$ field lies in the x-z plane. Since scattering will keep $\mathbf{H}$ pointing in the y direction, $E_y = 0$ everywhere, turning this problem into a two dimensional one. When we define the total electric field $\mathbf{E}$ as the solution to this scattering problem, the scattered field $\mathbf{E}^s$ can be found from $\mathbf{E}^i = \mathbf{E} - \mathbf{E}^s$.

B. The integral equation in the spatial domain

For $e^{j\omega t}$ time convention, the integral equation can be written as the combination

$$\begin{aligned}\mathbf{E}^i(x,z) =& \mathbf{E}(x,z) - \mathbf{E}^s(x,z) = \mathbf{E}(x,z) - \\ & \int_{-W}^{W} dx' \int_{z_{min}}^{z_{max}} dz' \, \frac{k_0^2}{j\omega\varepsilon_0\varepsilon_{rb,i}} \mathcal{G}(x,z|x',z') \cdot \mathbf{J}(x',z') \\ \mathbf{J}(x,z) =& j\omega\varepsilon_0\varepsilon_{rb,i}\chi(x,z)\mathbf{E}(x,z),\end{aligned} \tag{2}$$

where the $\mathcal{G}$ denotes the rank-two Green-function tensor in x and z, $\mathbf{J} = (J_x, J_z)$ defines the contrast current density and $k_0^2 = \omega^2\varepsilon_0\mu_0$ defines the squared wavenumber in vacuum. With the first of these equations we can compute the scattered field from the contrast current density. The integrals of the integral equation are in the form of a convolution with the Green tensor. The second equation will be called the field-material interaction.

In the x direction, the calculation of the scattered field can be handled most efficiently in the spectral domain, since there we can exploit the x-directed translation symmetry in the layered background medium. In the z direction, perpendicular to the layer interfaces, it is most convenient to work in the spatial domain, since there is no translation symmetry. For the field-material interaction we work in the spatial domain in both directions.

In the next sections we will first discuss the Green function operator (Section C). Then we describe how we discretize Eq. (2) (Section D) and afterwards we will explain how we can accurately compute the field material interaction (Section E).

C. The Green operator in the spectral domain

We use the Fourier transformation defined by

$$f(k_x) = \mathcal{F}_x[f(x)](k_x) = \int_{-\infty}^{\infty} dx \; f(x) e^{-jk_x x}. \tag{3}$$

In the spectral domain, we write functions with k_x as an argument and in the spatial domain with argument x. The Fourier transform of a function will be meant when the argument has changed from x to k_x and vice versa.

The Green operator can be written as a sum of two parts. The first part, $\mathcal{G}^h$, being the radiation into a homogeneous space with background dielectric constant $\varepsilon_{rb,i}$. The second part being the reflections at the layer interfaces. The scattered field due to the homogeneous part of the Green function can be written as

$$\mathbf{E}^h(k_x,z) = \frac{k_0^2}{j\omega\varepsilon_0\varepsilon_{rb,i}} \int_{z_{min}}^{z_{max}} dz' \; \mathcal{G}^h(k_x,z|z') \cdot \mathbf{J}(k_x,z), \tag{4}$$

where the homogeneous Green function is given by

$$\mathcal{G}^h(k_x,z|z') = -\begin{pmatrix} k_0^2\varepsilon_{rb,i} - k_x^2 & jk_x\partial_z \\ jk_x\partial_z & k_0^2\varepsilon_{rb,i} + \partial_z^2 \end{pmatrix} \frac{e^{-\gamma|z-z'|}}{2\gamma k_0^2}, \tag{5}$$

with $\gamma^2 = k_0^2 - k_x^2$. Note how we can identify a propagating part $e^{-\gamma|z-z'|}$ in $\mathcal{G}^h$, that governs how the electric field propagates over a distance $|z-z'|$ in the z direction.

The second part of the Green operator adds the reflections, originating from the layer interfaces, to the scattered electric

field, i.e.

$$\frac{k_0^2}{j\omega\varepsilon_0\varepsilon_{rb,i}}(\mathcal{G}\circ\mathbf{J})(k_x,z) = \mathbf{E}^s(k_x,z) = \mathbf{E}^h(k_x,z) + \left(\mathcal{R}^{u,u}(k_x)\cdot\mathbf{E}^h(k_x,z_{min}) + \mathcal{R}^{u,d}(k_x)\cdot\mathbf{E}^h(k_x,z_{max})\right)e^{-\gamma(z-z_{min})} + \left(\mathcal{R}^{d,d}(k_x)\cdot\mathbf{E}^h(k_x,z_{max}) + \mathcal{R}^{d,u}(k_x)\cdot\mathbf{E}^h(k_x,z_{min})\right)e^{-\gamma(z_{max}-z)}. \tag{6}$$

Here the $\mathcal{R}^{\alpha,\beta}$ denote the effective reflection coefficients, see [15] Chapter 5, from the layers below and above layer i including the offsets $z_{min}-z_i$ and $z_{max}-z_{i+1}$. Here $\beta = u/d$ (up/down) denotes the z propagation direction of the wave which generates the reflection and α denotes the direction in which the reflection itself propagates [4].

D. Discretization and spectral path

For discreatization in the x-direction we employ the Gabor frame as defined in [16] Chapter 8, with Gaussian window function

$$g(x) = 2^{\frac{1}{4}}e^{\left(-\pi\frac{x^2}{X^2}\right)}, \tag{7}$$

where X defines the width of the window function. For better convergence, rational oversampling by a factor $1/\alpha\beta$ is employed, with the Gabor frame defined by

$$g_{mn}(x) = g(x-m\alpha X)e^{jn\beta Kx}, \tag{8}$$

where $K = 2\pi/X$, the spectral step. To calculate Gabor coefficients, we use the dual frame found from the Moore-Penrose inverse [16, 17]. More details on the use of Gabor frames as a discretization for integral equations can be found in [4, 18].

Following the approach of [13, 19, 20], we use piecewise-linear expansion functions in the z direction

$$\Lambda_n(z) = \begin{cases} 1-\frac{|z-n\Delta-z_{min}|}{\Delta} & \text{if} \quad |z-n\Delta-z_{min}|<\Delta \\ 0 & \text{if} \quad |z-n\Delta-z_{min}|>\Delta \end{cases}. \tag{9}$$

For the test functions we use Dirac delta functions at $z = n\Delta + z_{min}$. In [20] it is explained how the z'-intergral in Eq. (4) can be computed efficiently.

In the x direction we use the Gabor frame as a basis and its dual to test, as explained in [18]. There it is also explained that in the spectral domain we do not represent functions on the real axis, but instead on the path, $\tau\in\mathbb{R}$,

$$k_x(\tau)\in\begin{cases}\tau - jA & \text{if } \tau<-A \\ (1+j)\tau & \text{if } -A\le\tau<A \\ \tau+jA & \text{if } \tau>A\end{cases}. \tag{10}$$

For A we choose a fixed value such that $AW\approx 3$. When a function $f(x)$ is transformed to the spectral domain, it is split up in $f_L(k_x)$, $f_M(k_x)$ and $f_R(k_x)$, each corresponding to the subsequent cases in Eq. (10). For $f_L(k_x)$ and $f_R(k_x)$ we use Gabor frames to represent these functions and for the middle part $f_M(k_x)$ we use a Taylor series. Since A is small compared to the total spectral range in which information is contained, the middle part contains little information and the Taylor series can be truncated after a few terms.

E. The field-material interaction

The main difficulty encountered in the TM scattering problem compared to the TE scattering problem is that the electric field has discontinuities wherever the contrast function has discontinuities. The electric field for TE scattering is continuous, so there we do not encounter this problem.

For RCWA it was pointed out in [5–7] that the convergence of a spatial-domain multiplication of two functions with a discontinuity at the same position is poor. In a spectral basis, such as in RCWA, this spatial multiplication is represented in the spectral domain by a convolution. When both functions have a spatial discontinuity, their spectral convergence is poor and the convergence of their convolution cannot be guaranteed. Wherever the contrast function is discontinuous, the electric field also has a discontinuous component, which leads to poor convergence in the field-material interaction in Eq. (2).

Although we use the Gabor frame instead of a Fourier series as a discretization, the same convergence problem comes into play. A function $f(x)$ represented by a set of Gabor coefficients f_{mn} can be written as

$$f(x) = \sum_{m=-\infty}^{\infty}\sum_{n=-\infty}^{\infty} f_{mn}g(x-m\alpha X)e^{jn\beta Kx} = \sum_{m=-\infty}^{\infty}\mathring{f}_m(x)g(x-m\alpha X), \tag{11}$$

with

$$\mathring{f}_m(x) = \sum_{n=-\infty}^{\infty} f_{mn}e^{jn\beta Kx}. \tag{12}$$

Now $\mathring{f}_m(x)$ is the resulting periodic function of the Fourier series in n, so a Gabor-frame representation can be seen as a collection in m of Fourier series in n. If $f(x)$ is discontinuous, then also (some of) the $\mathring{f}_m(x)$ are discontinuous. For a spatial multiplication, products with $\mathring{f}_m(x)$ are required and therefore again poor convergence is obtained with the Gabor frame when both functions have discontinuities at the same locations. In Figure 2 we illustrate this effect for a Heaviside stepfunction. We use the tilde here to denote a truncated Gabor-approximation of a function. Since the the Heaviside step function $H(x)$ equals its square: $H(x) = H^2(x)$, no noticable difference should be visible between the Gabor approximated $\tilde{H}$ and the Gabor approximated square $\widetilde{\tilde{H}*\tilde{H}}$. Obviously, there is a significant difference visible in Figure 2, hence the multiplication of discontinuous functions represented by Gabor coefficients is not accurate. An important difference is that the location of the step has shifted to the right. When applied to the field-material interaction, this would lead to a significantly smaller contrast current density and therefore to inaccurate results. For a good approximation these functions should overlap, since the same discretization is used on both. Although this example is different from the example used in [7], it is obvious that a significant error is made in the multiplication of discontinuous functions.

A reformulation of the problem is possible such that only one function is discontinuous [6, 12, 13, 21]. Let us consider a rectangular scatterer that is aligned with the layer interfaces. The electric-field component normal to a material interface is discontinuous and the electric field parallel to the interface is continuous. However, the electric flux density $\mathbf{D} = \varepsilon_r\varepsilon_0\mathbf{E}$ normal to a material interface is continuous, whereas the electric flux density parallel to the interface is discontinuous [22], Section 1.5. According to the Li-rules [7], we should select the con-

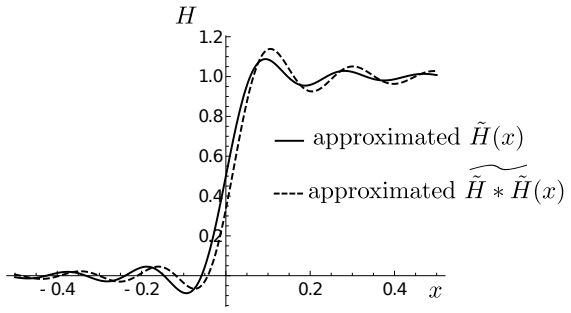

Fig. 2. Step functions approximated by Gabor coefficients truncated to $m \in -6,\ldots,6$ and $n \in -6,\ldots,6$ in a Gabor frame with $X = 1$ and $\alpha = \beta = \sqrt{2/3}$. Solid line: a direct approximation of the step function. Dashed line: An approximation of the square of the Gabor-represented step function, computed by a truncated convolution.

tinuous components. Let us assume the scattering from a rectangular object aligned with the coordinates. The discontinuity at the top and the bottom of the rectangle can be dealt with in the spatial z discretization. However, at the left and right side of the rectangle, $E_x(x,z)$ is discontinuous along the x coordinate and therefore the Li-rules are violated, so poor convergence can be expected for these interfaces. Now $D_x(x,z)$ and $E_z(x,z)$ are continuous at the sides of the of the rectangle

To address the problem of convergence we define the field $\mathbf{F}(x,z) = \hat{\mathbf{x}} D_x(x,z)/\varepsilon_0\varepsilon_{rb,i} + \hat{\mathbf{z}} E_z(x,z)$. We can calculate the electric field from $\mathbf{F}$ by

$$\mathbf{E} = \mathcal{L}_\chi \cdot \mathbf{F} = \begin{pmatrix} \frac{1}{1+\chi} & 0 \\ 0 & 1 \end{pmatrix} \cdot \mathbf{F} \tag{13}$$

and

$$\mathbf{J} = \mathcal{M}_\chi \cdot \mathbf{F} = \begin{pmatrix} 1 - \frac{1}{1+\chi} & 0 \\ 0 & \chi \end{pmatrix} \cdot \mathbf{F}. \tag{14}$$

Following the notation in [12], we rewrite Eq. (2) in a single equation as

$$\mathbf{E}^i = \mathcal{L}_\chi \cdot \mathbf{F} + -k_0^2 \mathcal{G} \circ (\mathcal{M}_\chi \cdot \mathbf{F}). \tag{15}$$

In the next section this formulation will be shown to converge much better when we use Gabor frames in the x direction compared to the case where the Li-rules have been ignored, i.e. when we choose

$$\mathcal{L}_\chi = \mathrm{Id} \tag{16}$$

$$\mathcal{M}_\chi = \chi\,\mathrm{Id}, \tag{17}$$

with Id the 2×2 identity matrix. We note that more general objects can in principle be treated by using normal-vector fields [8, 9, 23, 24].

3. RESULTS

A. Accuracy

We have validated the above outlined algorithm against the JCMWave software package [25] for two different usecases. We aimed for a relative accuracy of 10^{-3}, since engineering parameters like the material properties are often determined with less or similar precision for most practical applications. The simulation parameters were chosen with this criterion in mind and optimized for speed. The first usecase, Figure 3(a), consists of two

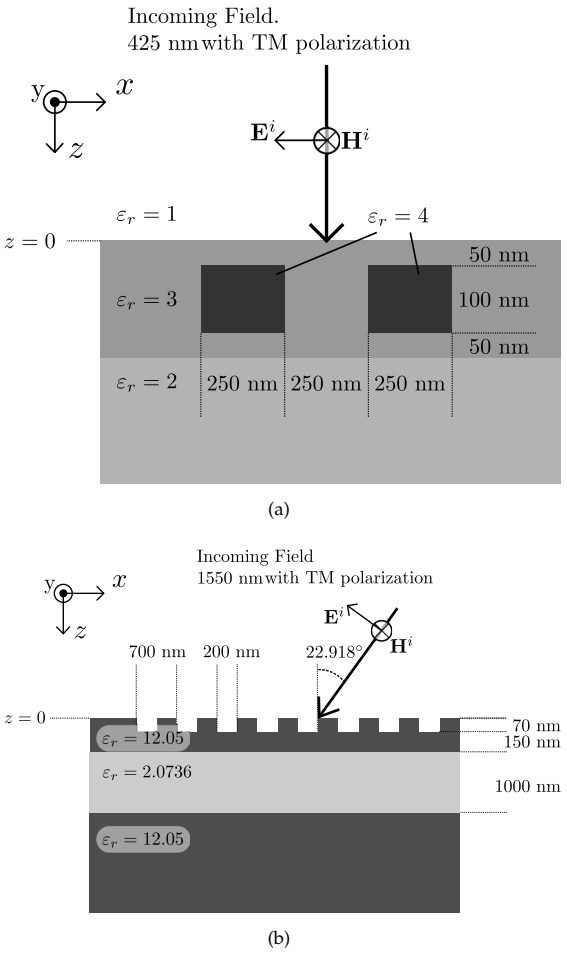

Fig. 3. (a) The first use case consists of two blocks in a layered medium. (b) A grating coupler consisting of grooves in a thin high-contrast medium on top of a thick low-contrast layer.

blocks in a layered medium. This is a relatively low-contrast case, since the difference in relative permitivity between the background, $\varepsilon_{rb,1} = 3$, and the blocks, with $\varepsilon_r = 4$, is small.

Figure 4 presents the real part of the scattered electric field $\mathbf{E}^s(x,z)$ for the geometry in Fig. 3 (a) excited by a plane wave of unit amplitude. The first figure represents the x-directed component of the electric field and the second figure shows the z-directed component. For this simulation we used one piecewise-linear basis function (Eq. (9)) per 2.5 nm in the z direction. In the x direction a Gabor frame was chosen with $X = 250$ nm in Eq. (7), $\alpha = \beta = \sqrt{3/2}$ in Eq. (8), and index $m \in \{-5,\ldots,5\}$ and index $n \in \{-6,\ldots,6\}$ in Eq. (8), totalling 143 Gabor coefficients in the x direction, equaling one coefficient per 15.7 nm on a simulation domain at some distance around the object. We chose the discretization in both x- and z-directions such that it contributed approximately the same error to the end result. Clearly, the Gabor coefficients in the x direction are more efficient in accurately discretizing the problem than the piecewise-linear functions in the z direction. We used 40% extra Gabor coefficients in the spectral domain for a finer sampling of the auxiliary field in Eq. (4).

Figure 5 shows the error with respect to JCMWave for the case in Figure 3 (a), in Figure (a) and (b) through the middle of the blocks at $z = 100$ nm, and in (c) and (d) at $z = 10$ nm, just be-

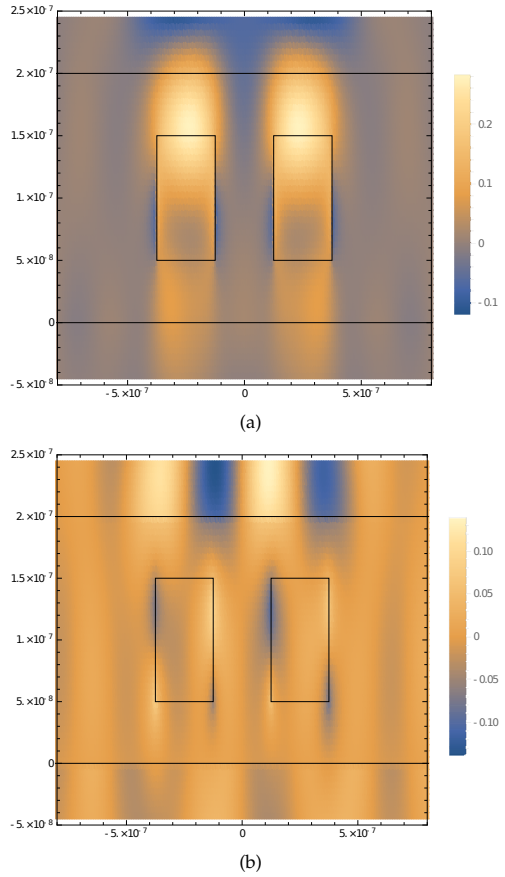

Fig. 4. The real part of (a) the scattered electric field in the x-direction and (b) the electric field in the z-direction

low the upper interface. Results with the auxiliary field formulation (Eq. (13) and Eq. (14)) and without the auxiliary field formulation (Eq. (16) and Eq. (17)) are shown, so they can be compared. In Figure 5 (a) we show the electric field $E_{x,V}(x, 100\text{nm})$ from the JCMWave validation, $F_x(x, 100\text{nm})/(1+\chi(x, 100\text{nm}))$ from the presented algorithm with auxiliary field formulation, and $E_x(x, 100\text{nm})$. It is clear that the accuracy found using the auxiliary field formulation is much better, although we observe some Gibbs ringing in the auxiliary field formulation as well in Figure 5(b). The discontinuity of the dielectric object induces the Gibbs phenomenon on the solution. Since this Gibbs error has a very high frequency, it does not radiate very far away from the blocks. For example, in scattering calculations this error does not contribute to the long-distance scattering. On the blocks, the Gibbs phenomenon dominates the error, but at a distance the Gibbs ringing is attenuated, so only the error that really radiates dominates there. In Figures 5 (c) and (d) we have plotted the electric field 10 nm below the upper layer. Here the Gibss phenomenon does not play a role anymore and the results obtained using the auxiliary field formulation (Eq. (13) and Eq. (14)) have a relative accuracy better than 10^{-3}. However, without the auxiliary-field formulation, the error is at least two orders of magnitude larger.

The second usecase, Figure 3(b), was inspired by [3], where several setups for grating couplers with TE polarization were introduced. We have chosen the grating coupler geometry and angle of incidence such that it couples TM waves efficiently into the same multilayer medium. However, the geometry was not

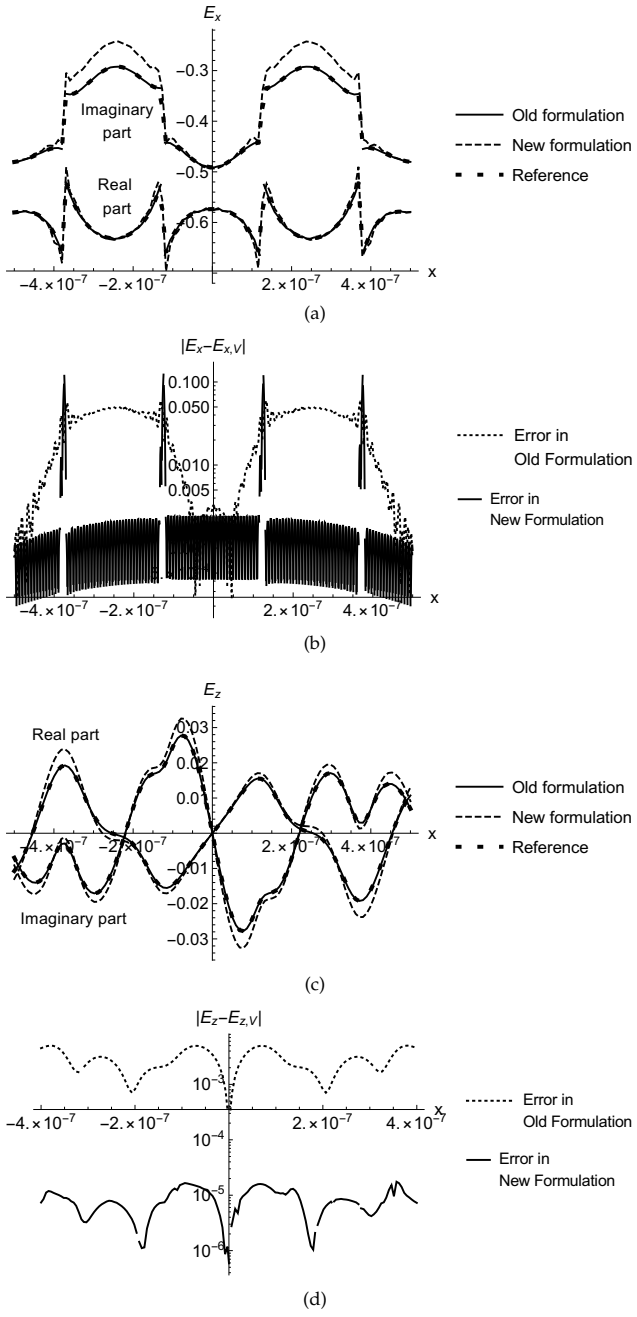

Fig. 5. The electric field for the case in Figure 3 (a). In (a),(b) it is E_x at $z = 100$ nm and in (c),(d) it is E_z at $z = 10$ nm. (a),(c) show field strength. With old formulation we mean results obtained without the auxiliary field formulation (Eq. (16) and Eq. (17)), and with the new formulation the described algorithm with auxiliary field formulation **F** is meant (Eq. (13) and Eq. (14)). (b),(d) show the difference between simulation and reference.

optimized for optimal coupling to the same degree as in the original article.

The electric field of the second testcase is presented in Figure 6 for excitation by a plane wave of unit amplitude. It can be clearly seen that the incoming waves couple to a right-travelling wave trapped within the 220 nm high-contrast layer. Since the simulation domain can be limited to the grooves in the multilayer medium, the simulation domain was chosen from $z = 0$ tot $z = 70$ nm in 15 piecewise-linear expansion functions, equalling one basis function per 4.6 nm. In the x direction a Gabor frame was chosen with $X = 1550$ nm in Eq. (7), $\alpha = \beta = \sqrt{3/2}$ in Eq. (8), and index $m \in \{-7, \ldots, 7\}$ and index $n \in \{-40, \ldots, 40\}$ in Eq. (8), totalling 1215 Gabor coefficients in the x direction, equalling one coefficient per 15.6 nm on a simulation domain around the object.

These results were also validated using JCMWave. In Figure 6 (c), the difference between JCMWave and results obtained with the present algorithm are shown. The results obtained with the auxiliary field formulation (Eq. (13) and Eq. (14)) agree well up to a level of 10^{-3}, however, the iterative solver did not converge to even 1 digit precision in 300 iterations for the formulation without auxiliary field (Eq. (16) and Eq. (17)), whereas the auxiliary field formulation converged in fewer than 25 iterations with BiCGStab(2) [26]. We calculated the error from the field strengths at the lower side of the high-contrast layer at $z = 220$nm to reduce the Gibbs ringing. From this we can conclude that the amplitude of the wave coupled into the layer agrees with the JCMWave results for the auxiliary field formulation.

B. Computation time

To see how the computation time of our algorithm scales to a finer discretization, we have refined both the discretization in the x direction and the z direction, while keeping the discretization in the other direction constant. Figure 7 shows that the computation time scales as $O(N_z)$ in the z-direction, with N_z the number of piecewise-linear basis function in the z direction, starting from the reference at $N_z = 21$ piecewise-linear functions. The same figure also shows an $O(N_x \log N_x)$ dependence with N_x corresponding to the range of n in the number of included Gabor frame functions (Eq. (8)), starting from the reference $N_x = 143$ frame functions.

4. CONCLUSION

We have succesfully reformulated the two-dimensional TM scattering problem for finitely sized dielectric scatterers in a dielectric layered medium with a volume integral equation in a mixed spatial and spectral basis in terms of a continuous auxiliary field $\mathbf{F}$ (Eq. (13) and Eq. (14)), which leads to a satisfactory convergence. A formulation without such a continuous field (Eq. (16) and Eq. (17)), which violates the Li-rules, shows much poorer accuracy in one test case and in the other test case convergence of the iterative solver was not reached.

We showed numerical evidence that the computation time scales as $O(N_x N_z \log N_x)$ with respect to refinements in the discretization.

For two cases we have shown that the proposed algorithm, that employs a discretization on a path through the complex spectral plane, combined with a Gabor frame, can be used for TM polarization.

This algorithm is capable of characterizing both the scattering from dielectric objects and the coupling of waves into a di-

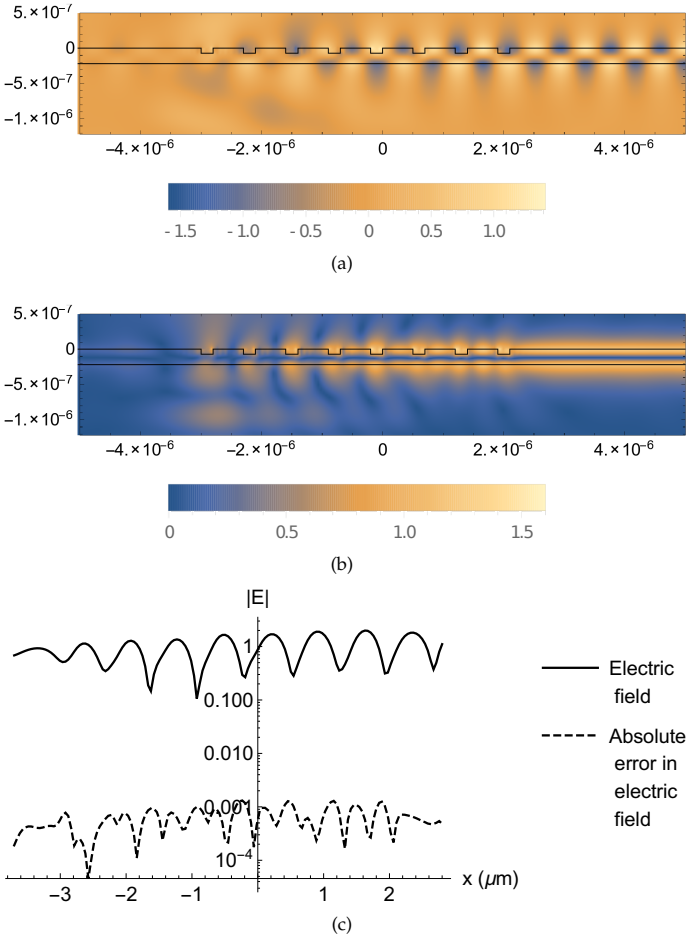

Fig. 6. The x-directed scattered field $E_x^s(x, z)$ for an incoming field of unit amplitude; (a) the real part, (b) the absolute value, (c) top line: the $|E|$ field at $z = 220$nm, bottom line: the absolute difference with the JCMWave results.

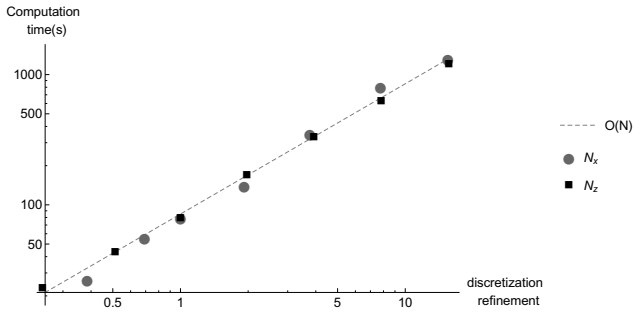

Fig. 7. Scaling of the computation time for the case in Figure 3 (a), with on the x axis the factor with which the numbers of unknowns N_x and N_z were increased compared to the results in Figure 4 and Figure 5, where $N_x = 143$ unknowns and $N_z = 21$ unknowns.

electric layer via a grating coupler.

REFERENCES

1. Y.-S. Ku, H.-L. Pang, W. Hsu, and D.-M. Shyu, "Accuracy of diffraction-based overlay metrology using a single array target," Optical Engineering (2009).
2. S. Jahani and Z. Jacob, "All-dielectric metamaterials," Nature Nanotechnology **11**, 23–36 (2016).
3. D. Taillaert, F. V. Laere, M. Ayre, W. Bogaerts, D. V. Thourhout, P. Bienstman, and R. Baets, "Grating couplers for coupling between optical fibers and nanophotonic waveguides," Japanese Journal of Applied Physics **45**, 6071–6077 (2006).
4. R. J. Dilz and M. C. van Beurden, "An efficient complex spectral path formulation for simulating the 2D TE scattering problem in a layered medium using Gabor frames," Journal of Computational Physics **345**, 528–542 (2017).
5. P. Lalanne and G. M. Morris, "Highly improved convergence of the coupled-wave method for TM polarization," Journal of the Optical Society of America A (1996).
6. G. Granet and B. Guizal, "Efficient implementation of the coupled-wave method for metallic lamellar gratings in TM polarization." Journal of the Optical Society of America A (1996).
7. L. Li, "Use of Fourier series in the analysis of discontinuous periodic structures," Journal of the Optical Society of America A **13**, 1870–1876 (1996).
8. E. Popov and M. Nevière, "Maxwell equations in Fourier space: fast-converging formulation for diffraction by arbitrary shaped, periodic, anisotripc media," Journal of the Optical Society of America A (2001).
9. T. Schuster, J. Ruoff, N. Kerwien, S. Rafler, and W. Osten, "Normal vector method for convergence improvement using the RCWA for crossed gratings," Journal of the Optical Society of America A (2007).
10. I. C. Botten, M. S. Craig, R. C. McPhedran, J. L. Adams, and J. R. Andrewartha, "The dielectric lamellar diffraction grating," Optica Acta **28**, 413–428 (1981).
11. M. G. Moharam and T. K. Gaylord, "Rigorous coupled-wave analysis of planar-grating diffraction," Journal of the Optical Society of America **73**, 452–455 (1981).
12. M. C. van Beurden, "Fast convergence with spectral volume integral equation for crossed block-shaped gratings with improved material interface conditions," Journal of the Optical Society of America A **28**, 2269–2278 (2011).
13. M. C. van Beurden, "A spectral volume integral equation method for arbitrary bi-periodic gratings with explicit Fourier factorization," Progress in Electromagnetics Research B **36**, 133–149 (2012).
14. M. Nevière, P. Vincent, R. Petit, and M. Cadilhac, "Systematic study of resonances of holographic thin film couplers." Optics Communications **9**, 48–53 (1973).
15. M. G. M. M. van Kraaij, "Forward diffraction modelling: Analysis and application to grating reconstruction," Ph.D. thesis, Eindhoven University of Technology (2011).
16. H. G. Feichtinger and T. Strohmer, *Gabor Analysis and Algorithms: Theory and Applications* (Birkhauser, 1998).
17. M. J. Bastiaans, "Gabor's expansion and the Zak transform for continuous-time and discrete-time signals: Critical sampling and rational oversampling," (1995).
18. R. J. Dilz and M. C. van Beurden, "The Gabor frame as a discretization for the 2D transverse-electric scattering-problem domain integral equation," Progress in Electromagnetics Research B **69**, 117–136 (2016).
19. I. Gohberg and I. Koltracht, "Numerical solution of integral equations, fast algorithms and Krein-Sobolev equation," Numerical Mathematics **47**, 237–288 (1985).
20. Y.-C. Chang, G. Li, H. Chu, and J. Opsal, "Efficient finite-element, Green's function approach for critical-dimension metrology of three-dimensional gratings on multilayer films," Journal of the Optical Society of America A (2006).
21. M. C. van Beurden, "Scattering by periodic dielectric media via a spectral domain-integral equation: maintaining efficiency and accuracy," in "Proceedings of the 2011 International Conference on Electromagnetics in Advanced Applications (ICEAA)," (2011), pp. 967–968.
22. J. D. Jackson, *Classical Electrodynamics* (Wiley, 2007).
23. T. J. Coenen and M. C. van Beurden, "A spectral volume integral method using geometrically conforming normal-vector fields," Progress in Electromagnetics Research (2013).
24. M. C. van Beurden, T. J. Coenen, and I. D. Setija, "Parametric modeling of doubly periodic dielectric structures via a spectral-domain integral equation," in "Proceedings of the 2013 International Conference on Electromagnetics in Advanced Applications (ICEAA)," (2013).
25. S. Burger, L. Zschiedrich, J. Pomplun, and F. Schmidt, "Finite-element based electromagnetic field simulations: benchmark results for isolated structures," in "Proc. SPIE 8880 Photomask Technology," , vol. 8880 (2013), vol. 8880.
26. H. A. van der Vorst, *Iterative Krylov Method for Large Linear Systems* (Cambridge University Press, 2003).